IEEE Access
Multidisciplinary : Rapid Review : Open Access Journal

Received 31 December 2022, accepted 13 January 2023, date of publication 18 January 2023, date of current version 24 January 2023.

Digital Object Identifier 10.1109/ACCESS.2023.3237825

RESEARCH ARTICLE

Improved Designs for Highly Integrated Lowpass–Bandpass Filters

PU-HUA DENG, (Member, IEEE), KUO-LUN SUN, JIA-HAN HSU, AND KAI-JIE XU
Department of Electrical Engineering, National University of Kaohsiung, Kaohsiung 811, Taiwan

Corresponding author: Pu-Hua Deng (phdeng@nuk.edu.tw)

This work was supported by the Ministry of Science and Technology, Taiwan, under Grant MOST 107-2221-E-390-007, Grant MOST 109-2221-E-390-018, and Grant MOST 110-2221-E-390-008.

ABSTRACT This study presents three dual-band lowpass–bandpass filters. The first handles lowpass and bandpass bands through its fifth-order and third-order Chebyshev filter responses, respectively. This filter uses three circuits to achieve flexibility in cutoff frequencies and fractional bandwidths. The second is a higher-order filter: it is a dual-band filter with ninth-order lowpass and fifth-order bandpass responses. In general, an extra 50-Ω transmission line might be required to connect each port conveniently to an external circuit for the first or second proposed filter, which could increase the circuit area. The third is a dual-band filter with a $\lambda/4$ impedance transformer near each port to facilitate connections with external circuits. Each of the proposed dual-band lowpass–bandpass filters has a systematic design procedure when the lowpass and bandpass band responses are given separately. In addition, the proposed filters can provide rapid prediction through the use of ideal circuit simulations instead of full-wave simulations.

INDEX TERMS Bandpass, Chebyshev, dual-band, filter, lowpass, systematic.

I. INTRODUCTION

Dual-band filters with bandpass responses in each passband were widely used [1], [2], [3], [4], [5], [6], [7], [8], [9], [10], [11], [12], [13]. To meet compact size requirements, [1] and [7] used ceramic lamination technique and printed circuit board to develop multilayered structures and [8] used meandering stepped-impedance resonators to reduce the sizes. Coupled-feed structures were used by [2] for dual-band external quality factors, and [3] designed dual-band transformer as a dual-band impedance match for each presented filter input or output port. A previous study [4] proposed dual-band coupling coefficients that could be independently designed, but external quality factors resulted in a complex disjointed design. Another study [6] designed dual-band filters with a properly arranged feeding structure that can achieve good spurious suppression response, but they needed extra impedance transformers. To avoid the additional transformers, dual-band external quality factors that can be satisfied through systematic direct-feed filter design were first proposed by [9], [10], [11], [12], and [13] introduced reconfigurable dual-band filters that changed their frequency responses depending on the biased circuit conditions.

Recently, lowpass–bandpass response multiband circuits, such as those presented by [14], [15], [16], [17], [18], [19], [20], [21], [22], [23], [24], [25], [26], [27], [28], [29], and [30], have been developed. Each of [14], [17], and [23] was lowpass-bandpass diplexer (LBD) for two different band channel application. In [17] and [23], the loading effect of the bandpass filter (BPF) circuit was overcome through the design of a suitable lowpass filter (LPF) structure. In contrast to [14], [17], and [23] used a directed-feed structure for BPF, and its input or output resonator was also shared to achieve the required shunt-to-ground capacitance of LPF, featuring a high circuit integration. A lowpass–bandpass triplexer (LBT) was proposed by [20], and [15], [16], [21], [24], [29], and [30] proposed dual-band lowpass–bandpass filters (DB-LBFs), triple-band lowpass–bandpass filters (TB-LBFs), and quad-/five-band lowpass–bandpass filter. A previous study [22] introduced a switchable lowpass–bandpass filter, and [18] presented reconfigurable DB-LBF that provided four-mode functions, with an independent design for LPF and BPF

The associate editor coordinating the review of this manuscript and approving it for publication was Giovanni Angiulli.

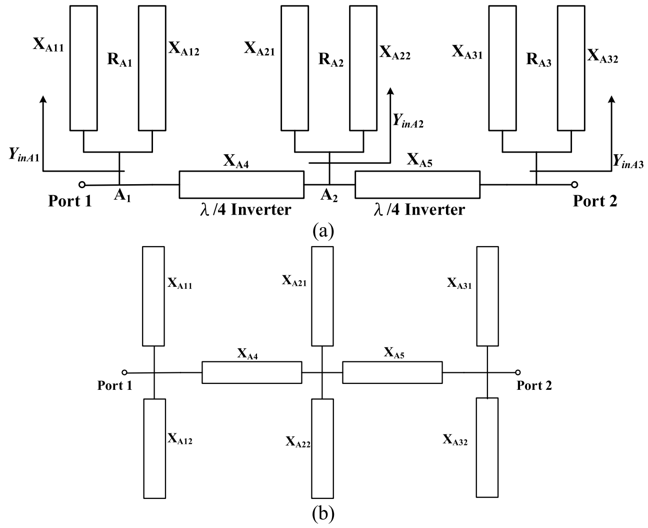

FIGURE 1. (a) LBF A structure and (b) its equivalent circuit.

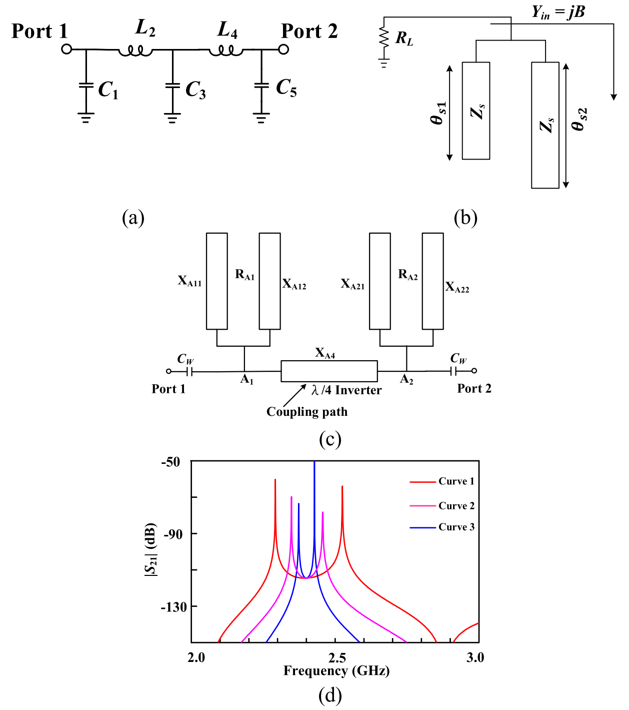

FIGURE 2. LBF A: (a) LPF band equivalent circuit, (b) input or output resonator structure, (c) coupling structure of resonators, and (d) coupling coefficients of resonators.

responses in an effective simplified design process. However, the DB-LBF required additional BPF resonators outside the LPF circuit, resulting in a low circuit integration or a large circuit size. In addition, [21] presented a highly integrated DB-LBF, with LPF and BPF sharing the same circuit; but its LPF and BPF responses could not be independently designed. For example, when one LPF or BPF response was indicated, the other response was determined under the indicated response; this design offered little flexibility. Furthermore, the f_0 (center frequency of the BPF response) to f_c (cutoff frequency of the LPF response) ratio was greater than 5, which might be unsuitable when the LPF band is close to the bandpass band. A previous study [24] used quasi-lumped elements to achieve the required capacitances and inductances for DB-LBFs. However, the device's equivalent circuit was complex, the parasitic effect of the lumped elements was insufficiently low, and extra chip capacitors for [24] were required, resulting in a complex design or possibly increasing circuit costs. Moreover, the LBF and BPF passbands featured the use of transmission zero locations in the design of their responses, which made it unsuitable for one to use familiar methods of synthesis, such as the Chebyshev method, to rapidly predict results; this approach failed to achieve a higher-order filter design. The synthesis issue was also faced in quasi-lumped circuits such as LPF [26], reconfigurable bandpass/lowpass filter [27], or triple-band lowpass–bandpass filter (TB-LBF) [29] design. In general, filters using lumped elements to approach their design responses can meet compact circuit size results. However, they usually need time-consuming optimization processes because of producing massive undesired parasitic effects. [30] used planner circuit design, but its equivalent circuit was complicated and it failed to provide the useful synthesis method such as the Chebyshev approach for designing higher-order DB-LBF responses.

To the best of our knowledge, little research has been conducted on DB-LBFs or reconfigurable DB-LBFs, and studies such as [15], [16], [21], [24], [27], and [30] have low circuit integration, parasitic effect issue, or complicated design issue. This study designed three types of DB-LBFs (LBF A, LBF B, and LBF C), each achieving the complete integration of LPF and BPF. The proposed DB-LBFs are also systematically designed when the specifications of LPF and BPF are independently indicated.

II. DESIGN OF LBF A

Fig. 1(a) presents the proposed LBF A structure. It is composed of eight transmission line sections, X_{A11}–X_{A32}, X_{A4}, and X_{A5}, with electric lengths of θ_{A11}–θ_{A32}, θ_{A4}, and θ_{A5}, respectively; the characteristic impedances are Z_{A11}–Z_{A32}, where $Z_{Ai1} = Z_{Ai2} = Z_{Ai}(i = 13)$, Z_{A4}, and Z_{A5}, respectively. Y_{inA1}–Y_{inA3} are input admittances. Fig. 1(a) can be redrawn to feature a bilateral symmetrical structure [Fig. 1(b)]. Fig. 2(a) is the fifth-order LPF equivalent circuit of LBF A with the same eight transmission lines (X_{A11}–X_{A32}, X_{A4}, and X_{A5}) in the design of its response. In Fig. 2(a), C_1, C_3, and C_5 are capacitances and L_2 and L_4 are inductances. The design equations of the LPF capacitances and inductances are as follows [31]:

$$C_k = \frac{g_k}{2\pi R_0 f_c}, \tag{1}$$

$$L_k = \frac{R_0 g_k}{2\pi f_c}, \tag{2}$$

where g_k, R_0, and f_c are the prototype element value, source impedance, and cutoff frequency, respectively. The coupled- resonator BPF response of the center frequency f_0 is formed using three resonators (R_{A1}, which comprises X_{A11} and X_{A12}; R_{A2}, which comprises X_{A21} and X_{A22}; and R_{A3}, which comprises X_{A31} and X_{A32}) and two inverters (X_{A4} and X_{A5}). The n-order coupled-resonator BPF design equations [31] are

$$Q_{ei} = \frac{g_0 g_1}{FBW}, \tag{3}$$

$$Q_{eo} = \frac{g_n g_{n+1}}{FBW}, \tag{4}$$

$$M_{ii+1} = \frac{FBW}{\sqrt{g_i g_{i+1}}}, \quad i = 1 - n, \tag{5}$$

where Q_{ei}/Q_{eo} is the external quality factor Q_L of the input or output resonator, n is the filter order number, $g_0 g_{n+1}$ denotes lowpass filter prototype lumped-element values, FBW is the fractional bandwidth variable, and M_{ii+1} is the coupling coefficient between two adjacent resonators. The λ/2 uniform impedance resonator (UIR) resonators $R_{A1}R_{A3}$ resonate at f_0 and are equivalent to three shunt-to-ground capacitors with the capacitances of C_1, C_3, and C_5, respectively, when their frequencies are at f_c. Furthermore, the feed-line locations of R_{A1} and R_{A3} are required to satisfy the external quality factors of (3) and (4), respectively. The external quality factor Q_L of a lossless resonator is also noted by [32] and written as

$$Q_L = \frac{R_L \omega_0}{2} \frac{\partial B}{\partial \omega}\Big|_{\omega=\omega_0}. \tag{6}$$

In (6), ω is the angular frequency variable, $\omega_0 = 2\pi f_0$ is the center angular frequency, R_L is the input impedance from the resonator looking into the load, and B is the susceptance of the input admittance Y_{in} from the feed point to the resonator. Fig. 2(b) illustrates the input or output λ/2 UIR structure that forms the basis of the external quality factor calculation, where Z_s and θ_s are the characteristic impedance and electrical length, respectively. By using (6), one can derive the external quality factor of Fig. 2(b) as follows:

$$Q_L = \frac{R_L}{2Z_s}[\theta_s \sec^2\theta_s + (180^\circ - \theta_s)\sec^2(180^\circ - \theta_s)]. \tag{7}$$

Because R_{A1} must satisfy the requisite Q_L through the use of (7) at f_0 and because its input admittance Y_{inA} equals the admittance of C_1 in Fig. 2(a) at ω_c ($\omega_c = 2\pi f_c$), the related design equations [23] can be written as

$$\begin{aligned} Q_L = \frac{Z_0}{2Z_{A1}}&[\theta_{A11}\sec^2\theta_{A11} \\ &+ (180^\circ - \theta_{A11})\sec^2(180^\circ - \theta_{A11})], \end{aligned} \tag{8}$$

$$\begin{aligned} Y_{inA1} = j\omega_c C_1 = j\frac{1}{Z_{A1}}&\tan\left(\frac{f_c}{f_0}\theta_{A11}\right) \\ &+ \tan\left[\frac{f_c}{f_0}(180^\circ - \theta_{A11})\right]. \end{aligned} \tag{9}$$

In (8) and (9), θ_{A11} is the electrical length at f_0 and Z_0 is the system impedance. The remaining two unknown variables, Z_{A1} and θ_{A11}, can be solved by (8) and (9) when the specifications of LPF and BPF are determined. LBF A is

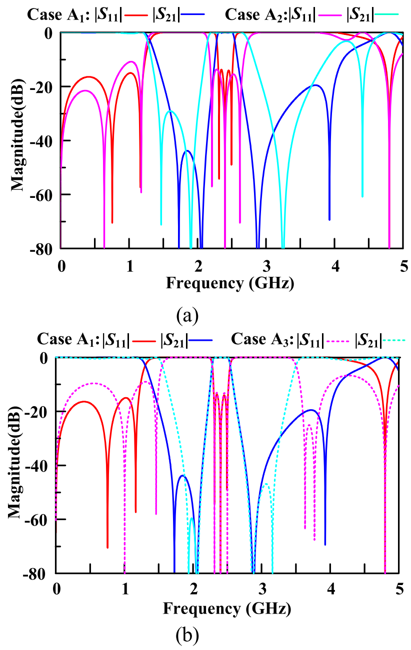

FIGURE 3. **Simulated results of LBF A ideal circuits. (a) Case A_1 and Case A_2. (b) Case A_1 and Case A_3.**

designed for fifth-order-LPF and third-order-BPF dual-band Chebyshev responses; LBF A has a bilateral symmetrical circuit and R_{A1} has the same design parameters as R_{A3}. Line section X_{A4} serves as a λ/4 inverter between R_{A1} and R_{A2} at f_0, and it approaches L_2 in Fig. 2(a) at f_c; this design is the same as that of line section X_{A5} because of the symmetrical property of LBF A. In practice, $f_c < f_0$ is optimal, f_c should not be too close to f_0, and the characteristic impedance of X_{A4} should not be low. The characteristic impedance $Z_{\lambda/4}$ of a λ/4 inverter [31] can be approached as

$$Z_{\lambda/4} \approx \frac{\omega_c L_k}{2\tan\left[45^\circ\left(\frac{f_c}{f_0}\right)\right]}. \tag{10}$$

Let $L_k = L_2$ in (10); this yields the characteristic impedance $Z_{A4} = Z_{\lambda/4}$ of X_{A4}. Furthermore, the connected-coupling technique of either [33] or [34] can be applied to make the coupling coefficients M_{12} be between R_{A1} and R_{A2} and M_{23} be between R_{A2} and R_{A3}; these are achieved using two connected lines: the first is X_{A4} and the second is X_{A5}. Fig. 2(c) demonstrates a coupling structure for R_{A1} and R_{A2}, where the capacitance $C_W = 0.001$pF models a weak coupling. For giving the LPF and BPF specifications, the required element values of Fig. 2(a) and Q_L in (3) and (4) are determined. To facilitate the design, the following steps are executed:

Step I[A]: The design of R_{A1} must satisfy the conditions of (8) and (9). Thus, R_{A1} can meet the required Q_L at f_0 and C_1 of Fig. 2(a) at f_c. The design parameters of R_{A3} are the same as those of R_{A1} because LBF A has a bilateral symmetrical structure. Thus, Q_L at f_0 and C_5 of Fig. 2(a) for R_{A3} can be simultaneously satisfied. Moreover, each length

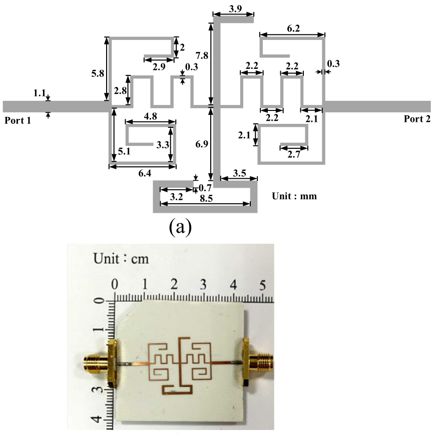

FIGURE 4. **Layout and photograph of Case A_1.**

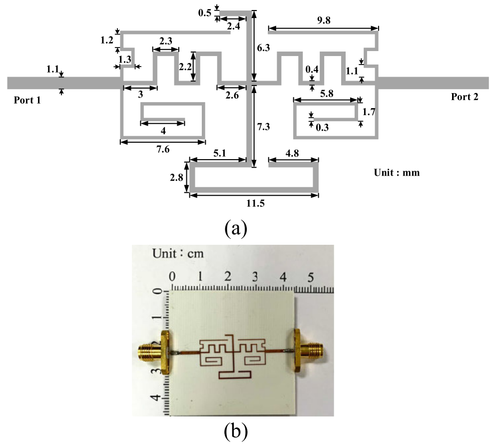

FIGURE 5. **Layout and photograph of Case A_2.**

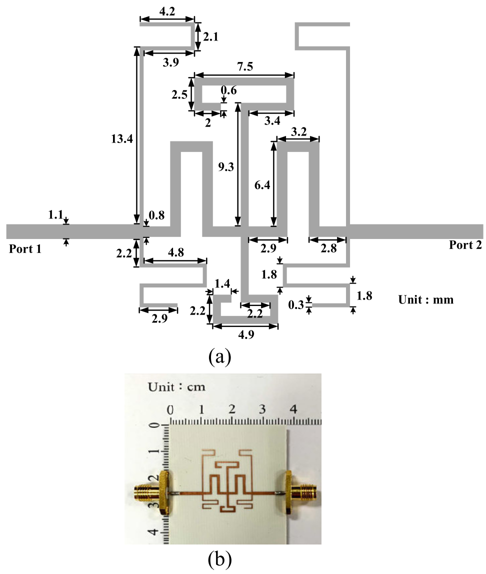

FIGURE 6. **Layout and photograph of Case A_3.**

of R_{A1}, R_{A2}, and R_{A3} is $\lambda/2$ at f_0, enabling each of them to reach resonance condition at f_0.

Step II^A: The characteristic impedances Z_{A4} of X_{A4} or Z_{A5} of X_{A5} can be designed using (10). Thus, L_2 and L_4 of LPF are met.

Step III^A: R_{A2} is $\lambda/2$ at f_0 to satisfy the BPF resonance condition, but it must still satisfy C_3 of Fig. 2(a) at f_c. The design equation is similar to that of (9) and can be written as

$$j\omega_c C_3 = j\frac{1}{Z_{A2}} \tan\left(\frac{f_c}{f_0}\theta_{A21}\right) + \tan\left[\frac{f_c}{f_0}\left(180^\circ - \theta_{A21}\right)\right], \tag{11}$$

where θ_{A21} is the electrical length of f_0. All the circuit parameters of R_{A1} have been determined in Steps I^A and II^A. C_3, f_c, and f_0 are identified when the response specifications of LPF and BPF are given. The remaining two design variables θ_{A21} and Z_{A2} are arbitrarily indicated one variable and the other variable can be solved using (11). The coupling coefficient between R_{A1} and R_{A2} is M_{12}, which can be designed by varying θ_{A21} and Z_{A2} in Fig. 2(c) to meet BPF specification using (5). Fig. 2(d) illustrates the different M_{12} simulations by changing θ_{A21} and Z_{A2} when $\theta_{A11} = 75^\circ$, $\theta_{A4} = 90^\circ$, $Z_{A1} = 90.27\Omega$, and $Z_{A4} = 82.76\Omega$ at f_0. The three responses are represented by Curve 1 ($\theta_{A21} = 45^\circ$ and $Z_{A2} = 71.6\Omega$), Curve 2 ($\theta_{A21} = 70^\circ$ and $Z_{A2} = 53.88\Omega$), and Curve 3 ($\theta_{A21} = 80^\circ$ and $Z_{A2} = 51.41\Omega$). For $\theta_{A21} < 90^\circ$ at f_0, M_{12} increases in magnitude as the length of θ_{A21} decreases. LPF and BPF responses of the proposed LBF A are fifth-order and third-order Chebyshev designs, respectively, $C_1 = C_5$, $L_2 = L_4$, $Q_{ei} = Q_{eo}$, and $M_{12} = M_{23}$. Thus, LBF A can achieve bilateral symmetry. Therefore, the design parameters of X_{A5} and R_{A3} are designed to be similar to those of X_{A4} and R_{A1}, respectively; this allows M_{23} to simultaneously meet the required value when M_{12} designed through the adjustment of the length of θ_{A21}.

By systematically following the procedure in Steps I^A–III^A, one can design the DB-LBF response of LBF A without undertaking the time-consuming task of optimizing the LPF and BPF responses. In this study, all the DB-LBFs were implemented on an RO4003C substrate with a thickness of 0.508 mm, loss tangent of 0.006, and dielectric constant of 3.58. LBF A has three circuits: Case A_1, Case A_2, and Case A_3. Table 1 summarizes the specifications of the three circuits.

Based on the design described in this section, the related design parameters can be obtained from Table 2 and the remaining parameters are also known because LBF A is a bilateral symmetrical circuit and R_{A1}–R_{A3} are UIRs. Fig. 3 illustrates simulated instances of Cases A_1–A_3 for comparison. A comparison of Case A_1 with Case A_2 [Fig. 3(a)] reveals the flexibility in the design of the BPF response fractional bandwidth at the same f_c and f_0 values, and a comparison of Case A_1 with Case A_3 [Fig. 3(b)] reveals the flexibility in the design of f_c at the same f_0 and BPF response fractional bandwidth values. The layouts and photographs of Cases A_1–A_3 are presented in Figs 4–6, and the simulation

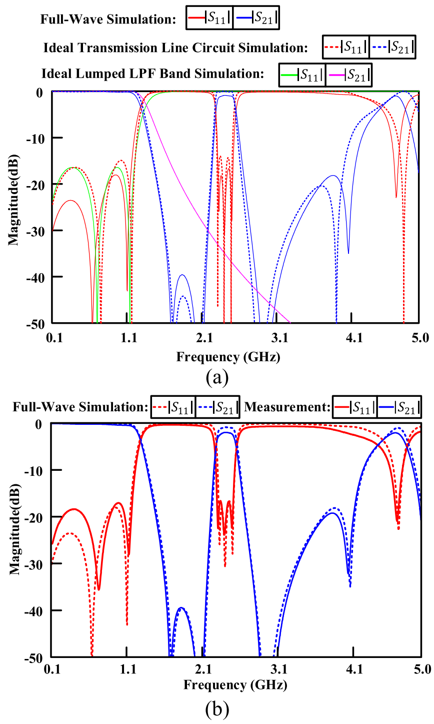

FIGURE 7. (a) Full-wave simulation, ideal transmission line circuit simulation, and ideal lumped LPF simulation of Case A_1;(b) full-wave simulation and measurement of Case A_1.

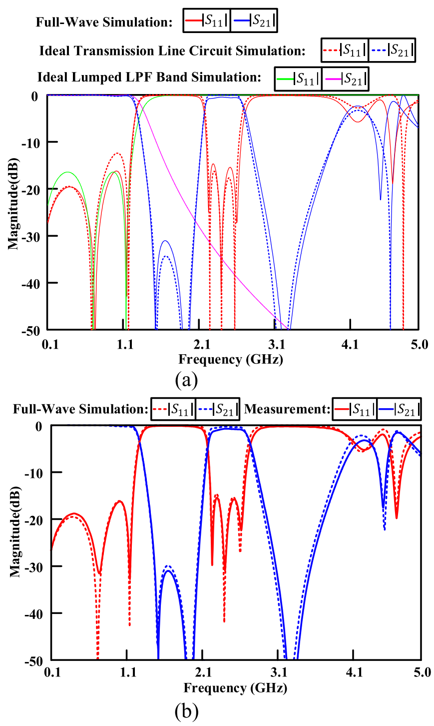

FIGURE 8. (a) Full-wave simulation, ideal transmission line circuit simulation, and ideal lumped LPF simulation of Case A_1;(b) full-wave simulation and measurement of Case A_2.

and measurement results are provided in Figs. 7–9. The different meander lines in Figures 4, 5, and 6 are just for compact

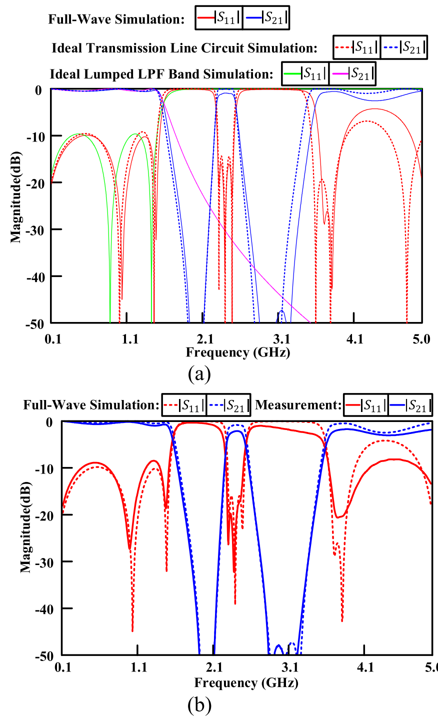

FIGURE 9. (a) Full-wave simulation, ideal transmission line circuit simulation, and ideal lumped LPF simulation of Case A_1;(b) full-wave simulation and measurement of Case A_3.

TABLE 1. Specifications of cases A_1–A_3.

	LPF response		BPF response		
	equal-ripple value (dB)	f_c (GHz)	equal-ripple value (dB)	f_0 (GHz)	FBW (%)
Case A_1	0.1	1.2	0.1	2.4	8
Case A_2	0.1	1.2	0.1	2.4	20
Case A_3	0.5	1.5	0.1	2.4	8

TABLE 2. Design parameters of cases A_1–A_3 at f_0 = 2.4GHz.

	θ_{A11}	θ_{A12}	θ_{A21}	θ_{A22}	θ_{A4}	Z_{A11}	Z_{A21}	Z_{A4}
Case A_1	75°	105°	55.4°	124.6°	90°	90.3 Ω	61.8 Ω	82.8 Ω
Case A_2	67.6°	112.4°	40°	140°	90°	94.3 Ω	78.8 Ω	82.8 Ω
Case A_3	75.4°	104.6°	69.3°	110.7°	90°	95.5 Ω	70.3 Ω	57.5 Ω

circuit area layouts and theses lines ignore their meander effects in circuit designs. For lowpass band, ideal lumped LPF simulation meets exactly required 0.1 dB equal-ripple value in Case A_1 or Case A_3; 0.5 dB equal-ripple value in Case A_2. Minor equal-ripple value errors for other lowpass or bandpass band responses in Figs. 7–9, which are caused by the approaching circuit designs or measured errors. Note that each BPF band has three ripples for each $|S_{11}|$ corresponding to third-order equal-ripple filter response. Table 3 lists the approximated measurement results.

III. DESIGN OF LBF B

The LBF B structure [Fig. 10(a)] is an example of a higher-order DB-LBF response; it is composed of 14 transmission line sections: X_{B11}–X_{B52} and X_{B6}–X_{B9}, with electrical

TABLE 3. Approximated measurement results of cases A_1–A_3.

	Lowpass band		BPF response		
	max. insertion loss (dB)	f_c (GHz)	min. insertion loss (dB)	f_0 (GHz)	3 dB FBW (%)
Case A_1	0.46	1.2	2	2.41	11
Case A_2	0.43	1.2	0.91	2.43	22.4
Case A_3	1	1.5	2.23	2.42	10.3

lengths of θ_{B11}–θ_{B52} and θ_{B6}–θ_{B9}, respectively. The characteristic impedances are Z_{B11}–Z_{B52}, where $Z_{Bi1} = Z_{Bi2} = Z_{Bi}(i = 15)$ and Z_{B6}–Z_{B9}, respectively. Y_{inB1}–Y_{inB3} are input admittances. Fig. 10(a) can be redrawn to feature a bilateral symmetrical structure [Fig. 10(b)]. The design of the ninth-order LPF Chebyshev response is based on these 14 transmission lines, with an equivalent circuit presented in Fig. 10(c). The coupled-resonator BPF response of the center frequency f_0 [31] is formed by five resonators R_{B1}–R_{B5}, with R_{Bi} comprising X_{Bi1} and X_{Bi2}, and four λ/4 inverters X_{B6}–X_{B9}. At f_c, R_{B1}–R_{B5} are also equivalent to the five shunt-to-ground capacitances C_1–C_9 of Fig. 10(c), respectively. Each of the λ/4 inverters X_{B6}–X_{B9} has a similar design to the λ/4 inverter X_{A4} in LPF A. The design procedure is summarized as follows:

Step I^B: The design of R_{B1} or R_{B5} is similar to that of R_{A1} in Step I^A.

Step II^B: At f_c, the four λ/4 inverters X_{B6}–X_{B9} are designed to satisfy the four series inductances L_2–L_8 of Fig. 10(c), respectively. A similar design as that in Step II^A is used for this step.

Step III^B: R_{B2} must simultaneously resonate at f_0 and achieve the shunt-to-ground capacitance C_3 [in Fig. 10(c)] at f_c, which has a similar design to R_{A2} in Step III^A. Because the designs of R_{B1} and X_{B6} are completed in Steps I^B and II^B, their circuit parameters are fixed. C_3, f_c, and f_0 are identified when the specifications of the LPF and BPF responses are determined. The corresponding Z_{B2} is obtained through adjustment of θ_{B21}, which can be used to design the required coupling coefficient M_{12} between R_{B1} and R_{B2}. Based on a similar design concept, R_{B3} resonates at f_0 and is also equivalent to the shunt-to-ground capacitance C_5 of Fig. 10(c). The parameters of R_{B2} and X_{B7} cannot be changed after the M_{12} and Step II^B designs are completed, respectively. The coupling coefficient M_{23} between R_{B2} and R_{B3} is designed by adjusting θ_{B31} given the corresponding Z_{B3}. Because LBF B has a bilateral symmetrical configuration, the design of the remaining parts is obtained.

LBF B, which has a Chebyshev ninth-order lowpass filter and fifth-order bandpass dual-band filter, is designed in its entirety by following Steps I^B–III^B systematically; this process does away with the need for the time-consuming task of optimizing the two desired bands. Compared with LBF A, LBF B achieves a higher-order DB-LBF response and can be extended to higher-order designs for DB-LBFs.

LBF B is designed for $f_c = 1.2$ GHz for a 0.1-dB equal-ripple LPF response and $f_0 = 2.4$ GHz and $FBW = 9\%$ for a 0.1-dB equal-ripple BPF response. Based on the

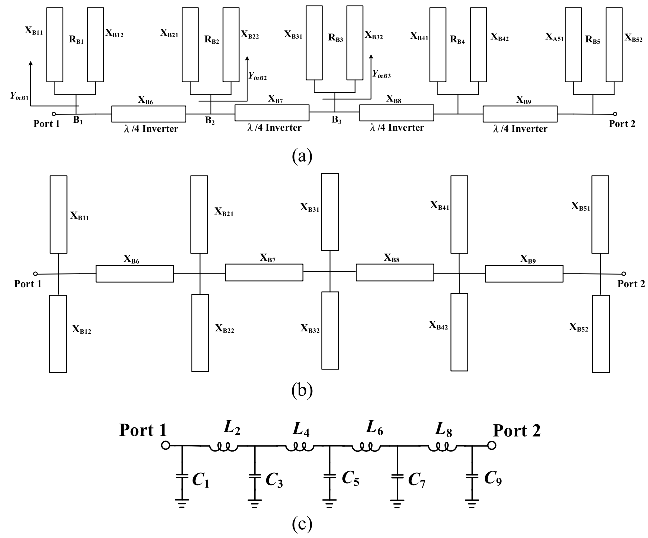

FIGURE 10. (a) LBF B structure, (b) its equivalent circuit, and (c) its LPF band equivalent circuit.

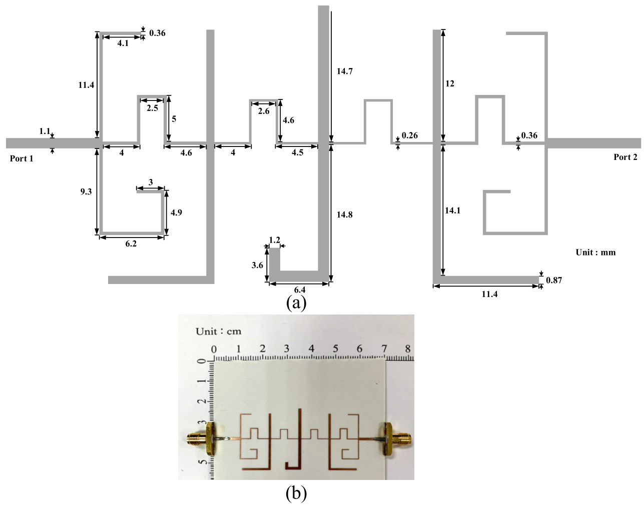

FIGURE 11. Layout and photograph of LBF B.

specifications, the related design parameters of f_0 are $\theta_{B11} = \theta_{B51} = 74.6°$, $\theta_{B12} = \theta_{B52} = 105.4°$, $\theta_{B21} = \theta_{B41} = 55°$, $\theta_{B22} = \theta_{B42} = 125°$, $\theta_{B31} = 72.5°$, $\theta_{B32} = 107.5°$, $\theta_{B6} = \theta_{B7} = \theta_{B8} = \theta_{B9} = 90°$, $Z_{B1} = Z_{B5} = 86.75\Omega$, $Z_{B2} = Z_{B4} = 57.19\Omega$, $Z_{B3} = 47.54\Omega$, $Z_{B6} = Z_{B9} = 87.07\Omega$, and $Z_{B7} = Z_{B8} = 97.58\Omega$. Fig. 11 details the layout and presents a photograph of LBF B, and the simulated and measured results are presented in Fig. 12. In the lowpass band, the measured passband maximum insertion loss and cutoff frequency are approximately 0.769 dB and 1.2 GHz, respectively; in the bandpass band, the measured passband minimum insertion loss, 3 dB FBW, and center frequency are approximately 2.98 dB, 8.3%, and 2.415 GHz, respectively. For lowpass band, ideal lumped LPF simulation meets exactly required 0.1 dB equal-ripple value. Minor equal-ripple value errors for other lowpass or bandpass band responses in Fig.12, which

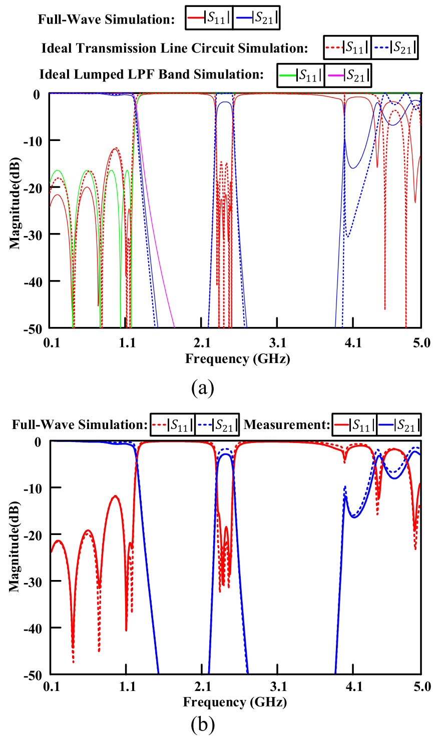

FIGURE 12. **(a) Full-wave simulation, ideal transmission line circuit simulation, and ideal lumped LPF simulation of LBF B;(b) full-wave simulation and measurement of LBF B.**

are caused by the approaching circuit design or measured errors.

IV. DESIGN OF LBF C

Fig. 13(a) presents the structure of LBF C with a DB-LBF response that improves the input or output circuit layout flexibility of the previously proposed filters in this study. LBF C has ten transmission line sections: X_{C11}–X_{C32} and X_{C4}–X_{C7}, with electrical lengths of θ_{C11}–θ_{C32} and θ_{C4}–θ_{C7}, respectively; the characteristic impedances are Z_{C11}–Z_{C32}, where $Z_{Ci1} = Z_{Ci2} = Z_{Ci} (i = 13)$ and Z_{C4}–Z_{C7}, respectively. Y_{inC1} and Y_{inC2} are input admittances, and Z_{inC4} is the input impedance. Fig. 13(a) can be redrawn to depict a bilateral symmetrical structure [Fig. 13(b)]. The ten transmission line sections with an equivalent circuit illustrated in Fig. 13(c) are used to design a seventh-order LPF Chebyshev response, where L_1–L_7 and C_2–C_6 are inductances and capacitances, respectively. Resonators R_{C1}–R_{C3} (R_{Ci} comprises X_{Ci1} and X_{Ci2}), two λ/4 inverters (X_{C5} and X_{C6}), and two λ/4 impedance transformers (X_{C4} and X_{C7}) are used to design the coupled-resonator BPF response [27] with center frequency f_0. The LBF C design procedure is as follows:

Step I^{C}: The length of X_{C4}–X_{C7} equals λ/4 at f_0 and satisfies the inductances L_1–L_7 of Fig. 13(c) at f_c when the specification of the dual-band Chebyshev lowpass and bandpass response is given. The characteristic impedances of X_{C4}–X_{C7} can be obtained using (10) and the specifications of theL_1–L_7 inductances.

Step II^{C}: Z_{C4} has been determined in Step I^{C}, and X_{C4} serves as the λ/4 impedance transformer at f_0. Thus,

$$Z_{in4} = \frac{Z_{C4}^2}{Z_0}, \tag{12}$$

where Z_0 is the system or load impedance of Port 1; Z_{in4} is solved using (12); and we then let $R_L = Z_{in4}$, $\theta_s = \theta_{C11}$, and $Z_S = Z_{C1}$ in (7). Therefore, the Q_L of R_{C1} at f_0 can be written as

$$Q_L = \frac{Z_{C4}^2}{2Z_{C1}Z_0}\left[\theta_{C11}\sec^2\theta_{C11} + \left(180^\circ - \theta_{C11}\right) \times \sec^2\left(180^\circ - \theta_{C11}\right)\right]. \tag{13}$$

The design of (13) is similar to that presented in [28]. Z_{C4} has been solved, $Z_0 = 50\Omega$ is the system impedance, and Q_L is identified using the given bandpass response specification. R_{C1} is equivalent to C_2 in Fig. 13(c) at f_C. Y_{inC1} at f_C is as follows:

$$Y_{inC1} = j\omega_c C_2 = j\frac{1}{Z_{C1}}\tan\left(\frac{f_c}{f_0}\theta_{C11}\right) + \tan\left[\frac{f_c}{f_0}\left(180^\circ - \theta_{C11}\right)\right]. \tag{14}$$

The two remaining unknown variables, Z_{C1} and θ_{C11}, can be obtained using (13) and (14) when the DB-LBF response specification is indicated.

Step III^{C}: R_{C2} simultaneously resonates at f_0 and must be equivalent to the shunt-to-ground capacitance C_4 of Fig. 13(c), which has the same design as R_{A2} in Step III^{A}. Because R_{C1} and X_{C5} are designed in Steps I^{C} and II^{C}, respectively, their parameters are fixed. For the DB-LBF response specification, C_3, f_c, and f_0 have been identified. Similar to what is done in Step III^{A}, the required coupling coefficient M_{12} between R_{C1} and R_{C2} can be achieved by changing the adjusted θ_{C21} to obtain the corresponding Z_{C2} value. Finally, the remaining design of LBF C is completed by virtue of its bilateral symmetry.

Each LBF A and LBF B port is at an input or output resonator. Thus, an additional $Z_0 = 50\Omega$ transmission line may be required at each port for ease of connection to other external circuits. X_{C4} or X_{C7} are included in LBF C and have a λ/4 length at f_0 to increase port layout flexibility and facilitate the connection to another circuit without the need for an additional Z_0 transmission line. By systematically following the LBF C design, one can achieve the required DB-LBF response without having to undertake any time-consuming processes.

LBF C is designed for $f_c = 1.2$GHz for a 0.1-dB equal-ripple LPF response and $f_0 = 2.4$GHz and $FBW = 9\%$ for a 0.1-dB equal-ripple BPF response. Based on the specifications, the related design parameters of f_0 are $\theta_{C11} = \theta_{C31} = 65^\circ$, $\theta_{C12} = \theta_{C32} = 115^\circ$, $\theta_{C21} = 57^\circ$, $\theta_{C22} = 123^\circ$, $\theta_{C4} = \theta_{C5} = \theta_{C6} = \theta_{C7} = 90^\circ$, $Z_{C1} = Z_{C3} = 77.55\Omega$, $Z_{C2} = 75.78\Omega$, $Z_{C4} = Z_{C7} = 71.29\Omega$, and $Z_{C5} = Z_{C6} = 126.55\Omega$. Fig. 14 depicts the layout and presents a photograph of LBF C, and the simulation and measurement results are

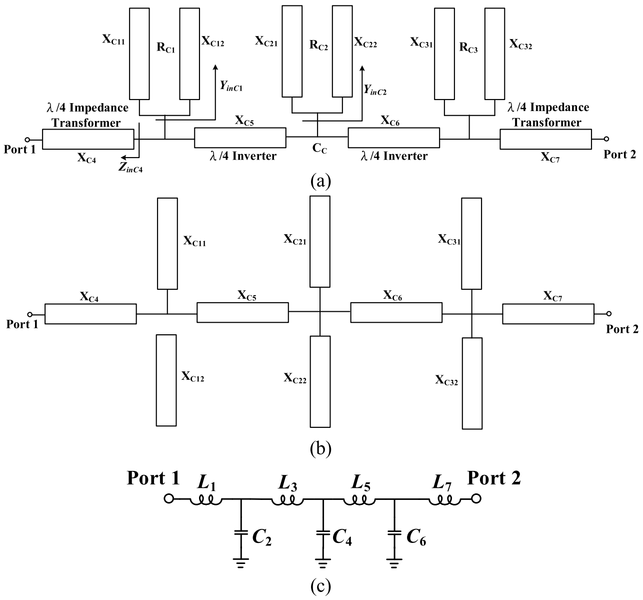

FIGURE 13. (a) LBF C structure, (b) its equivalent circuit, and (b) its LPF band equivalent circuit.

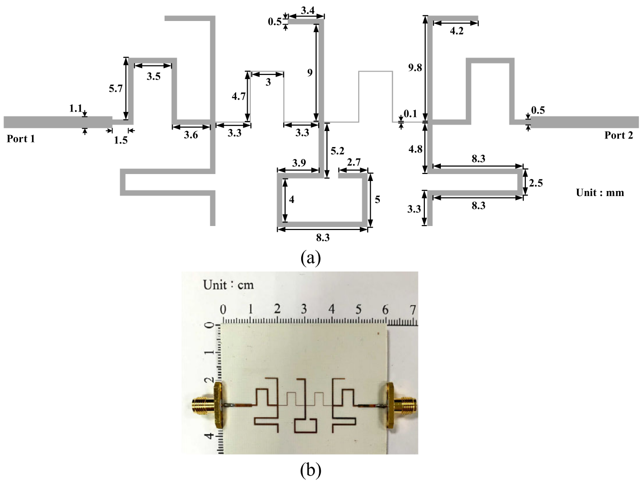

FIGURE 14. Layout and photograph of LBF C.

presented in Fig. 15. In the lowpass band, the measured passband maximum insertion loss and cutoff frequency are approximately 1.1 dB and 1.2 GHz, respectively; in the bandpass band, the measured passband minimum insertion loss, 3 dB *FBW*, and center frequency are approximately 1.684 dB, 12.2%, and 2.423 GHz, respectively. For lowpass band, ideal lumped LPF simulation meets exactly required 0.1 dB for the first or second equal-ripple value, but its third ripple is shifted approximately from 1.075 GHz (0.1 dB value) to 0.993 GHz (0.375 dB value), which error results from input or output transformer doesn't use enough high characteristic impedance to approach the required lumped inductance of LPF. However, it still achieves a satisfied initial LPF response design. Moreover, minor equal-ripple value errors for other lowpass or bandpass band responses in Fig.15, which are caused by the approaching circuit design or measured errors.

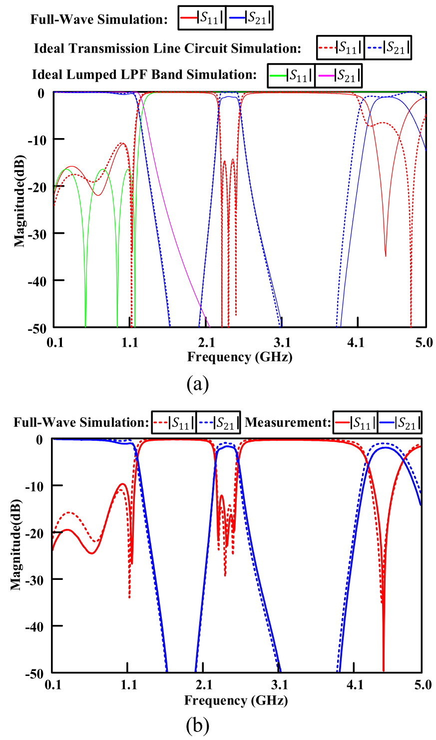

FIGURE 15. (a) Full-wave simulation, ideal transmission line circuit simulation, and ideal lumped LPF simulation of LBF C;(b) full-wave simulation and measurement of LBF C.

V. COMPARISON BETWEEN THE PROPOSED DB-LBFS AND THOSE IN THE LITERATURE

Table 4 lists the results for the proposed DB-LBFs and those from other studies for comparison. The DB-LBF in [21] could be designed using a synthesized method, such as in a Chebyshev response design; however, the lowpass and bandpass band specifications could not be independently indicated. Although the specification of the lowpass band was given and that of the bandpass band was determined, the proposed DB-LBFs provided separate dual-band specifications and could be systematically designed using the synthesized method. Even if Cases A_1–A_3 have higher filter orders, Cases A_1–A_3 were more compact than those in [16] and [15].

Compared with the proposed DB-LBFs, those in [24] were smaller; however, the circuits in [24] had fewer filter orders than those in the proposed circuits. Furthermore, [24] required a chip capacitor for the DB-LBF, which might increase circuit cost. The figure of merit (FOM) [26] for LPF response is defined as follows.

$$FOM = \frac{RSB \times \xi \times SF}{NSS}. \tag{15}$$

In (14), *RSB* is relative stopband bandwidth, ξ is roll-off-rate parameter, *SF* is suppression factor, and *NSS* is normalized structure size. The related FOM comparisons are also included in Table 4.

TABLE 4. Results for proposed DB-LBFs and those in the literature.

	DS	DSI	LO	BO	$f_c/f_0/F$	*FOM*	LI (dB)	BI (dB)	Size (λ_g^2)
Fig. 8(a) of [15]	N	N	3	2	3.3/7/ 27.3%	NI	NI	NI	0.176
Fig. 8(b) of [15]	N	N	3	2	4.6/9.3/ 15.1%	NI	NI	NI	0.184
[16]	N	N	3	2	4.1/7.3/ 4.5%	NI	NI	2	0.08
[21]	Y	N	5	5	1/5.2/ 38.5%	NI	0.5	0.8	0.7098
[24]	N	N	3	2	0.89/2.43/ 19.3%	NI	0.3	0.8	0.029
[30]	N	N	NI	NI	2.11/4.57/ 17.5%	NI	0.07	0.14	0.116
Case A_1	Y	Y	5	3	1.2/2.42/ 11%	4813.5	0.46	2	0.06978
Case A_2	Y	Y	5	3	1.2/2.44/ 10.4%	6375.6	0.43	0.91	0.06888
Case A_3	Y	Y	5	3	1.5/2.42/ 22.3%	2027.7	1	2.23	0.0655
LBF B	Y	Y	9	5	1.2/2.42/ 8.3%	4993.9	0.769	2.98	0.2189
LBF C	Y	Y	7	3	1.2/2.42/ 12.2%	3322.9	1.1	1.68	0.137

DS: designable using a synthesized method, such as in a Chebyshev response design; DSI: designable using a synthesized method after the dual-band specifications are independently given; LO: lowpass filter response order; BO: bandpass filter response order; *F*: 3-dB fractional bandwidth for all cases except the 0.8-dB fractional bandwidth for [21]; LI: lowpass band insertion loss; BI: bandpass band minimal or maximal insertion loss; λ_g: guided wavelength of a 50-Ω microstrip line at f_0 (GHz); f_c unit: GHz; Y: yes; N: no; NI: no information.

VI. CONCLUSION

This paper presents three DB-LBFs (LBF A, LBF B, and LBF C). The structure of LBF A boasts a flexible design, as is evident in the cutoff frequency for a lowpass band and the fractional bandwidth for a bandpass band. LBF B is also proposed as a higher-order DB-LBF. Finally, the LBF C structure can provide a flexible input or output layout to facilitate connection to an external circuit. These proposed DB-LBFs comprise transmission lines without any capacitive coupling structure; thus, the proposed circuits can provide rapid predictions through the use of ideal circuit simulations.

Furthermore, six transmission zeros in LBF A or LBF C and ten transmission zeros in LBF B, wherein each zero is produced by the corresponding open stub. The transmission zeros can improve the selectivity and stopband response of each proposed DB-LBF. Overall, each layout has an acceptable DB-LBF response below $|\pm 2\%|$ variation in the proposed fabricated circuit layout substrate. Specifically, LBF C has high characteristic impedance (126.55Ω)λ/4 inverter line causing its manufacturing sensitivity issue, which can be relaxed by using a thicker substrate. The performance of the circuits formulated in this study was also validated using simulations and empirical measurements.

REFERENCES

[1] H. Miyake, S. Kitazawa, T. Ishizaki, T. Yamada, and Y. Nagatomi, "A miniaturized monolithic dual band filter using ceramic lamination technique for dual mode portable telephones," in *IEEE MTT-S Int. Microw. Symp. Dig.*, Jun. 1997, pp. 789–792.
[2] S. Sun and L. Zhu, "Compact dual-band microstrip bandpass filter without external feeds," *IEEE Microw. Wireless Compon. Lett.*, vol. 15, no. 10, pp. 644–646, Oct. 2005.
[3] J.-T. Kuo, T.-H. Yeh, and C.-C. Yeh, "Design of microstrip bandpass filters with a dual-passband response," *IEEE Trans. Microw. Theory Techn.*, vol. 53, no. 4, pp. 1331–1337, Apr. 2005.
[4] C. F. Chen, T. Y. Huang, and R. B. Wu, "Design of dual- and triple-passband filters using alternately cascaded multiband resonators," *IEEE Trans. Microw. Theory Techn.*, vol. 54, no. 9, pp. 3550–3558, Sep. 2006.
[5] Y. P. Zhang and M. Sun, "Dual-band microstrip bandpass filter using stepped-impedance resonators with new coupling schemes," *IEEE Trans. Microw. Theory Techn.*, vol. 54, no. 10, pp. 3779–3785, Oct. 2006.
[6] J.-T. Kuo and H.-P. Lin, "Dual-band bandpass filter with improved performance in extended upper rejection band," *IEEE Trans. Microw. Theory Techn.*, vol. 57, no. 4, pp. 824–829, Apr. 2009.
[7] A. Djaiz, T. A. Denidni, and M. Nedil, "Dual-band filter using multi-layer structures and embedded resonators," *Electron. Lett.*, vol. 43, no. 9, pp. 527–528, Apr. 2007.
[8] Q. X. Chu and F. C. Chen, "A compact dual-band bandpass filter using meandering stepped impedance resonators," *IEEE Microw. Wireless Compon. Lett.*, vol. 18, no. 5, pp. 320–322, May 2008.
[9] P. H. Deng and H. H. Tung, "Design of microstrip dual-passband filter based on branch-line resonators," *IEEE Microw. Wireless Compon. Lett.*, vol. 21, no. 4, pp. 200–202, Apr. 2011.
[10] G. L. Dai and M. Y. Xia, "Design of compact dual-band switchable bandpass filter," *Electron. Lett.*, vol. 45, no. 10, pp. 506–507, May 2009.
[11] P.-H. Deng and J.-H. Jeng, "A switched reconfigurable high-isolation dual-band bandpass filter," *IEEE Microw. Wireless Compon. Lett.*, vol. 21, no. 2, pp. 71–73, Feb. 2011.
[12] M. L. Chuang and M. T. Wu, "Switchable dual-band filter with common quarter-wavelength resonators," *IEEE Trans. Circuits Syst. II, Exp. Briefs*, vol. 62, no. 4, pp. 347–351, Apr. 2015.
[13] Y.-H. Cho, C. Park, and S.-W. Yun, "0.7–1.0-GHz switchable dual-/single-band tunable bandpass filter using a switchable J-inverter," *IEEE Access*, vol. 9, pp. 16967–16974, 2021.
[14] M. H. Capstick, "Microstrip lowpass-bandpass diplexer topology," *Electron. Lett.*, vol. 35, no. 22, pp. 1958–1960, Oct. 1999.
[15] M. Awida, A. Balalem, A. Safwat, H. El-Hennawy, and A. Omar, "Combined low-pass and bandpass filter response using microstrip dual-mode resonators," in *IEEE MTT-S Int. Microw. Symp. Dig.*, Jun. 2006, pp. 701–704.
[16] M. Awida, A. Boutejdar, A. Safwat, H. El-Hennawy, and A. Omar, "Multi-bandpass filters using multi-armed open loop resonators with direct feed," in *IEEE MTT-S Int. Microw. Symp. Dig.*, Jun. 2007, pp. 913–916.
[17] P.-H. Deng and J.-T. Tsai, "Design of microstrip lowpass-bandpass diplexer," *IEEE Microw. Wireless Compon. Lett.*, vol. 23, no. 7, pp. 332–334, Jul. 2013.
[18] P.-H. Deng, J.-T. Tsai, and R.-C. Liu, "Design of a switchable microstrip dual-band lowpass-bandpass filter," *IEEE Microw. Wireless Compon. Lett.*, vol. 24, no. 9, pp. 599–601, Sep. 2014.
[19] J. Xu, "Compact microstrip tri-band lowpass-bandpass filter," *Electron. Lett.*, vol. 51, no. 19, pp. 1509–1510, Sep. 2015.
[20] F.-C. Chen, J.-M. Qiu, H.-T. Hu, Q.-X. Chu, and M. J. Lancaster, "Design of microstrip lowpass-bandpass triplexer with high isolation," *IEEE Microw. Wireless Compon. Lett.*, vol. 25, no. 12, pp. 805–807, Dec. 2015.
[21] F. C. Chen and Q. Shao, "Low insertion loss microstrip dualband lowpass-bandpass filter with controllable passband frequencies," *Microw. Opt. Technol. Lett.*, vol. 58, no. 8, pp. 1858–1861, Aug. 2016.
[22] P. K. Singh, A. K. Tiwary, and N. Gupta, "Ultra-compact switchable microstrip band-pass filter–low-pass filter with improved characteristics," *Microw. Opt. Technol. Lett.*, vol. 59, no. 1, pp. 197–201, Jan. 2017.
[23] P.-H. Deng, R.-C. Liu, W.-D. Lin, and W. Lo, "Design of a microstrip low-pass-bandpass diplexer using direct-feed coupled-resonator filter," *IEEE Microw. Wireless Compon. Lett.*, vol. 27, no. 3, pp. 254–256, Mar. 2017.
[24] J. Xu, Z. Y. Chen, and Q. H. Cai, "Design of miniaturized dual-band low-pass–bandpass and bandpass filters," *IEEE Trans. Compon., Packag., Manuf. Technol.*, vol. 8, no. 1, pp. 132–139, Jan. 2018.

[25] J. Xu, H. Wan, J. Q. Ding, and Y. X. Zhu, "Miniaturised tri-band lowpass–bandpass filter using lumped-element structure," *Electron. Lett.*, vol. 55, no. 5, pp. 272–274, Mar. 2019.
[26] D. K. Choudhary, M. A. Abdalla, and R. K. Chaudhary, "Compact D-CRLH resonator for low-pass filter with wide rejection band, high roll-off, and transmission zeros," *Int. J. Microw. Wireless Technol.*, vol. 11, nos. 5–6, pp. 509–516, Jun. 2019.
[27] M. A. Abdalla, D. K. Choudhary, and R. K. Chaudhary, "A compact reconfigurable bandpass/lowpass filter with independent transmission zeros based on generalized NRI metamaterial," *Int. J. RF Microw. Comput.-Aided Eng.*, vol. 30, no. 3, pp. 1–9, Nov. 2019.
[28] J. Xu, Z.-Y. Chen, and H. Wan, "Lowpass-bandpass triplexer integrated switch design using common lumped-element triple-resonance resonator technique," *IEEE Trans. Ind. Electron.*, vol. 67, no. 1, pp. 471–479, Jan. 2020.
[29] D. K. Choudhary and R. K. Chaudhary, "Compact lowpass and dual-band bandpass filter with controllable transmission zero/center frequencies/passband bandwidth," *IEEE Trans. Circuits Syst. II, Exp. Briefs*, vol. 67, no. 6, pp. 1044–1048, Jun. 2020.
[30] A. Kumar and D. K. Upadhyay, "Zig-zag monofilar spiral shaped CRLH TL based compact lowpass mono-/duo-/tri-/quad-bandpass filter," *IETE J. Res.*, May 2022, pp. 1–11.
[31] J. S. Hong and M. J. Lancaster, *Microstrip Filters for RF/Microwave Applications*. New York, NY, USA: Wiley, 2001.
[32] J.-T. Kuo and E. Shih, "Microstrip stepped impedance resonator bandpass filter with an extended optimal rejection bandwidth," *IEEE Trans. Microw. Theory Techn.*, vol. 51, no. 5, pp. 1554–1559, May 2003.
[33] T. N. Kuo, S. C. Lin, C. H. Wang, and C. H. Chen, "New coupling scheme for microstrip bandpass filters with quarter-wavelength resonators," *IEEE Trans. Microw. Theory Techn.*, vol. 56, no. 12, pp. 2930–2935, Dec. 2008.
[34] S.-C. Lin and T.-L. Jong, "Microstrip bandpass filters with various resonators using connected- and edge-coupling mechanisms and their applications to dual-band filters and diplexers," *IEEE Trans. Microw. Theory Techn.*, vol. 60, no. 4, pp. 975–988, Apr. 2012.

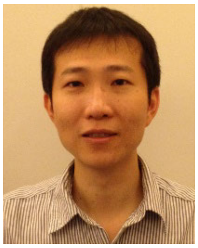

PU-HUA DENG (Member, IEEE) was born in Kaohsiung, Taiwan, in 1978. He received the B.Sc. degree in electrical engineering from National Sun Yet-sen University, Kaohsiung, in 2002, and the M.Sc. and Ph.D. degrees in communication engineering from National Taiwan University, Taipei, Taiwan, in 2004 and 2006, respectively.

In 2006, he joined ZyXEL Communication Corporation, Hsinchu, Taiwan, where he was a RF Engineer. In 2007, he joined NXP Semiconductors Company, Kaohsiung, where he was an Advanced RF Testing Engineer. From August 2008 to January 2009, he joined as a Faculty Member of the Department of Electrical Engineering, National University of Tainan, Tainan, Taiwan, as an Assistant Professor. Since 2009, he has been joining as a Faculty Member of the Department of Electrical Engineering, National University of Kaohsiung, Kaohsiung, where he is currently a Professor. His research interests include the design and analysis of microwave planar circuits.

KUO-LUN SUN was born in Kaohsiung, Taiwan, in 1997. He received the B.S. degree in electrical engineering from the National University of Kaohsiung, Kaohsiung, in 2020, where he is currently pursuing the Ph.D. degree.

JIA-HAN HSU was born in Kaohsiung, Taiwan, in 1996. He received the B.S. degree in electrical engineering from the National University of Kaohsiung, Kaohsiung, in 2019, where he is currently pursuing the M.S. degree.

KAI-JIE XU was born in Pingtung, Taiwan, in 1998. He received the B.S. degree in electrical engineering from the National University of Kaohsiung, Kaohsiung, Taiwan, in 2020 and 2022, respectively.